CORA Cork Open Research Archive
Cartlann Taighde Oscailte Chorcaí

Title	Broadband semiconductor light sources operating at 1060 nm based on InAs:Sb/GaAs submonolayer quantum dots
Authors	Herzog, B.;Lingnau, Benjamin;Kolarczik, M.;Helmrich, S.;Achtstein, A. W.;Thommes, K.;Alhussein, F.;Quandt, D.;Strittmatter, A.;Pohl, U. W.;Brox, O.;Weyers, M.;Woggon, U.;Lüdge, Kathy;Owschimikow, N.
Publication date	2019-05-29
Original Citation	Herzog, B., Lingnau, B., Kolarczik, M., Helmrich, S., Achtstein, A. W., Thommes, K., Alhussein, F., Quandt, D., Strittmatter, A., Pohl, U. W., Brox, O., Weyers, M., Woggon, U., Lüdge, K. and Owschimikow, N. (2019) 'Broadband Semiconductor Light Sources Operating at 1060 nm Based on InAs:Sb/GaAs Submonolayer Quantum Dots', IEEE Journal of Selected Topics in Quantum Electronics, 25(6), pp. 1-10. doi: 10.1109/JSTQE.2019.2919763
Type of publication	Article (peer-reviewed)
Link to publisher's version	https://ieeexplore.ieee.org/document/8725534 - 10.1109/JSTQE.2019.2919763
Rights	© 2019 IEEE. Personal use of this material is permitted. Permission from IEEE must be obtained for all other uses, in any current or future media, including reprinting/republishing this material for advertising or promotional purposes, creating new collective works, for resale or redistribution to servers or lists, or reuse of any copyrighted component of this work in other works.
Download date	2026-10-30 01:57:07
Item downloaded from	https://hdl.handle.net/10468/8393



University College Cork, Ireland
Coláiste na hOllscoile Corcaigh

This article has been accepted for publication in a future issue of this journal, but has not been fully edited. Content may change prior to final publication. Citation information: DOI 10.1109/JSTQE.2019.2919763, IEEE Journal of Selected Topics in Quantum Electronics

Broadband semiconductor light sources operating at 1060 nm based on InAs:Sb/GaAs submonolayer quantum dots

Bastian Herzog, Benjamin Lingnau, Mirco Kolarczik, Sophia Helmrich, Alexander W. Achtstein, Kevin Thommes, Fuad Alhussein, David Quandt, André Strittmatter, Udo W. Pohl, Olaf Brox, Markus Weyers, Ulrike Woggon, Kathy Lüdge, and Nina Owschimikow

***Abstract*—In this paper, we investigate the potential of submonolayer-grown InAs:Sb/GaAs quantum dots as active medium for opto-electronic devices emitting in the 1060 nm spectral range. Grown as multiple sheets of InAs in a GaAs matrix, submonolayer quantum dots yield light-emitting devices with large material gain and fast recovery dynamics. Alloying these structures with antimony enhances the carrier localization and red-shifts the emission, while dramatically broadening the optical bandwidth. In a combined experimental and numerical study, we trace this effect to an Sb-induced bimodal distribution of localized and delocalized exciton states. While the former do not participate in the lasing process, they give rise to a bandwidth broadening at superluminescence operation and optical amplification. Above threshold laser properties like gain and slope efficiency are mainly determined by the delocalized fraction of carriers.**

***Index Terms*—Quantum dots, Semiconductor materials, Semiconductor lasers, Semiconductor Optical Amplifiers**

I. Introduction

Arsenide-based quantum confined nanostructures are well established as gain media in opto-electronics, in particular as two-dimensional (2D) multiple-quantum wells which feature a high modal gain and spectrally narrow emission line, and can be customized by conveniently controllable growth parameters [1]. For high-speed applications, the growth of self-assembled quantum dots (QDs) gives access to a fast and temperature-stable yet not as bright broad-band active medium [2]–[5]. The potential to retain the advantages of zero-dimensional (0D) confinement, while simultaneously realizing a high material gain, motivated the growth of InAs/GaAs submonolayer (SML) QDs, essentially hybrid 0D-2D nanostructures with a much higher areal density than can be achieved with self-assembled QDs [6]–[10]. Opto-electronic devices based on SML QDs show a high modal gain, very fast gain recovery and large optical nonlinearities, at emission wavelengths typically shorter than 1000 nm [11]–[13].

A red-shift and general broadening of the SML QD emission is achieved by alloying with antimony (SML:Sb), enabling devices which cover the technologically important spectral range around 1060 nm [14]. This spectral range is of high interest e.g. for short-haul optical communication, due to the local absorption minimum of water around that particular wavelength. First steps towards the realization of mode-locked devices based on SML QDs have been recently demonstrated [15]. Another major application of broadband emitters around this particular wavelength is optical coherence tomography (OCT) in materials science or medical imaging [16]–[18]. Here, the bandwidth of the light source limits the depth resolution. As such procedures are becoming more widespread, it is important to optimize size, lifetime and energy efficiency of the devices employed. Owing to the high density of carrier localization centers and small overall dimensions of the In-rich sheets, InAs SML QDs feature a high material gain of about 1000 cm^{-1} per layer, as we will show later in this work. Antimony alloying leads to even smaller SML QDs and consequently a still higher material gain, accompanied by broadening of the emission spectrum. While static optical properties of SML:Sb QDs have previously been reported [14], [19], in our work we focus on the SML QDs as a gain medium in semiconductor devices such as lasers (SCLs) and amplifiers (SOAs), emitting in the 1060 nm optical range.

In this contribution the electronic structure of the SML:Sb material is investigated. From low temperature photoluminescence experiments we derive a numerical model to extract density of states and scattering mechanisms into and within the potential landscape. In a second part, we analyze SML:Sb based SCLs with respect to optical gain, emission spectra, and output power characteristics. The last part treats the SML:Sb-based SOAs, where we analyze response bandwidth, gain dynamics and amplitude phase coupling. To highlight the unique features of the SML:Sb QD material, we compare all device properties with reference samples based on a single layer of pure InAs/GaAs SMLs or a single quantum well (SQW) with comparable waveguide structures and designed to emit in the same wavelength range.

II. Samples and Experiment

The key idea of the SML growth is the formation of a high density of tailored localization centers. This is achieved by the deposition of InAs sheets as a submonolayer superlattice into a GaAs matrix, yielding InAs-rich islands inside an InGaAs quantum well. The main tuning parameters for number and depth of the potential traps are the nominal thickness of the InAs and GaAs layers [20]–[23]. Over a wide range of growth parameters the localized carrier wavefunctions have been found to form a dissimilar electron

1077-260X (c) 2019 IEEE. Personal use is permitted, but republication/redistribution requires IEEE permission. See http://www.ieee.org/publications_standards/publications/rights/index.html for more information.

This article has been accepted for publication in a future issue of this journal, but has not been fully edited. Content may change prior to final publication. Citation information: DOI 10.1109/JSTQE.2019.2919763, IEEE Journal of Selected Topics in Quantum Electronics

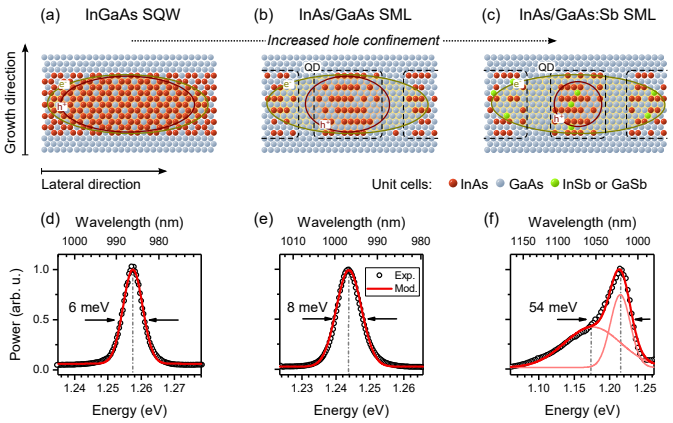


Fig. 1. Schematic structure of the (a) SQW, (b) SML and (c) SML:Sb active media (not to scale). (d) - (f) Respective photoluminescence spectra at 4 K sample temperature after optical excitation into the GaAs barrier. Solid lines: single (SQW, SML) and double-Gaussian (SML:Sb) fits to the data. Vertical lines mark the respective peak positions.

and hole confinement with localized holes and the electron wavefunctions extending over several neighboring InAs-rich islands [24]. Since In-adatoms tend to segregate during InAs growth on GaAs [13], an increase of the material contrast between In-rich and In-poor areas is a challenging issue. Adding small amounts of Sb adatoms between the growth cycles reduces the In mobility and thus enables the formation of islands with higher In-content gradients and reduced volume expansion [25], leading to enhanced carrier localization [26]. The combined effect of Sb inclusion is a general broadening and red-shift of the optical emission spectra of these structures, in particular the latter being highly desirable for applications in opto-electronics and medical imaging [16], [18].

Fabrication of SML QDs implies the choice of many growth parameters. This and the effect of various device designs makes a comparison with devices based on other quantization structures difficult. For our study, *pin* structures containing an InGaAs SQW, or single layers of pure InAs SML QDs or Sb-alloyed InAs SML QDs were grown using metalorganic vapor phase epitaxy (MOVPE), with the composition of all structures designed to achieve 1060 nm emission wavelength (1.17 eV) at room temperature. Figs. 1 (a) - (c) schematically show the epitaxial structures in terms of the respective lattice-unit cells. The structures change from regularly distributed InAs and GaAs in case of the (a) SQW up to In-rich agglomeration of InAs decreasing in size from the (b) SML to the (c) SML:Sb material. Solid circles sketch the exciton wavefunction primarily defined by the 2D extended electrons, dashed circles mark the shrinkage of the hole wavefunction from (a) to (c). Note that the respective carrier confinement potentials change from similar for electron and hole for the SQW up to dissimilar for the SML:Sb sample with larger extent for the electron [14], [24].

The layer structures of all devices contain a single active QW or QD layer with a 10 nm GaAs buffer to ensure comparable carrier pathways after electrical injection. The waveguides are each formed by a 300 nm $Al_{0.13}Ga_{0.87}As$ core inside an $Al_{0.30}Ga_{0.70}As$ cladding. The wafers were processed into photoluminescence (PL) samples as well as edge-emitting ridge waveguide lasers (SCLs) or optical amplifiers (SOAs) using identical processing masks for best comparability. All devices are designed for transverse single-mode emission and contain a 500 μm long waveguide. The active layer of the SML sample was grown using 15 cycles of nominally 0.73 ML InAs and 1.13 ML GaAs. For the SML:Sb sample we used an 8-fold deposition of nominally 0.83 ML InAs and 1.59 ML GaAs with a flush of 7 μmol Sb in between each growth cycle. The SQW reference sample contains an 8.3 nm thick $In_{0.23}Ga_{0.77}As$ SQW. All wafers were processed into light-emitting devices with straight and as-cleaved or angled and anti-reflection coated facets to obtain lasers or optical amplifiers, respectively. A waveguide width of nominally 3 μm of the shallow-etched devices ensured single-mode waveguiding. For the PL samples, the top *p*-side was removed by etching until the undoped $Al_{0.13}Ga_{0.87}As$ barrier of the active region was exposed.

For analysis of the temperature-dependent photoluminescence properties of the structures, samples were cleaved from the PL wafer sections and mounted in a helium-flow cryostat, allowing to vary the temperature between 4 K and room temperature. For the optical excitation at normal incidence, we used a mode-locked Ti:Sapphire laser emitting pulses of 250 fs duration with a repetition rate of 75.4 MHz to excite the samples above the GaAs band edge at 800 nm (1.55 eV). The laser power was limited to 300 μW (4 pJ/pulse) to avoid heating and saturation effects, corresponding to a maximum intensity of approximately 100 W/cm^2 on a 300 μm^2 spot on the sample. For the time-integrated detection we used a Horiba Jobin Yvon iHR 550 fully automated imaging spectrometer. The time-resolved measurement was realized by a Hamamatsu C5680 streak camera attached to an Acton2500 spectrometer with temporal and spectral resolutions of 33 ps and 0.5 nm, respectively.

For device characterization the edge-emitting SCLs and SOAs were glued on a copper submount, which was directly thermally coupled to a PID-controlled Peltier temperature control providing a thermal stabilization of $\Delta T < 0.2\ K$. The optical gain was determined via the Hakki-Paoli method [27] using short lasers of 0.5 mm length for best resolvability of the longitudinal cavity modes. The spectra were measured with an Hewlett Packard 70952B fiber-coupled optical spectrum analyzer at a spectral resolution of 0.08 nm. Measurements of gain and phase dynamics were performed with an heterodyne-detected pump probe setup according to Refs. [10] and [5].

III. Optical Properties

Photoluminescence spectra obtained at a temperature of 4 K from SQW, SML and SML:Sb samples upon optical excitation into the GaAs barrier are given in Figs. 1 (d) - (f), respectively. We observe a successive linewidth broadening from 6 meV for the SQW to 54 meV for the SML:Sb sample. The well-known lineshapes of the SQW and SML samples

1077-260X (c) 2019 IEEE. Personal use is permitted, but republication/redistribution requires IEEE permission. See http://www.ieee.org/publications_standards/publications/rights/index.html for more information.

This article has been accepted for publication in a future issue of this journal, but has not been fully edited. Content may change prior to final publication. Citation information: DOI 10.1109/JSTQE.2019.2919763, IEEE Journal of Selected Topics in Quantum Electronics

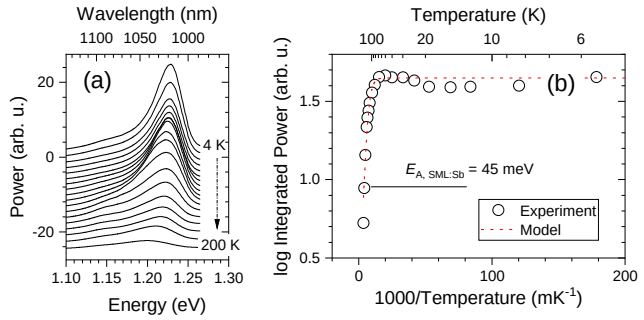


Fig. 2. (a) Photoluminescence spectra of the SML:Sb sample after optical excitation into the GaAs barrier with temperature increasing from 4 K to 200 K from top to bottom. (b) Arrhenius plot of the integrated peak power (symbols) and fit (line).

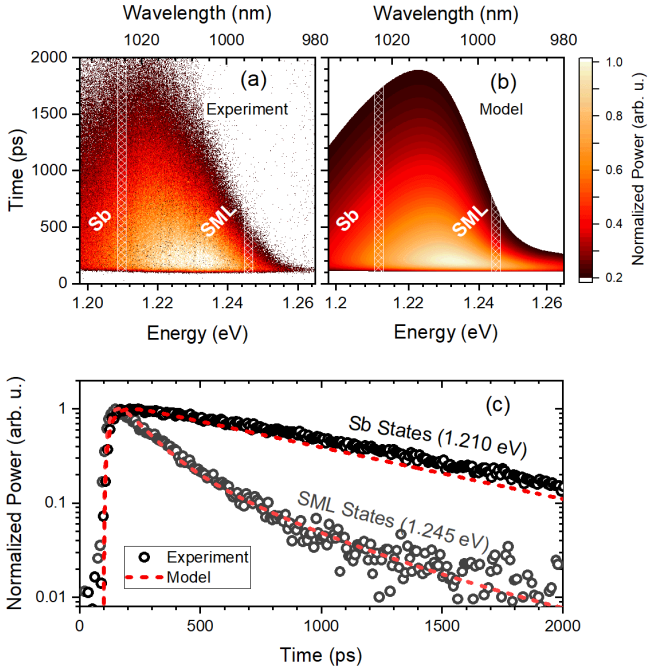


Fig. 3. Temporally and spectrally resolved photoluminescence of the SML:Sb sample at a temperature of 4 K and optical excitation into the GaAs barrier. (a) Measured data, (b) modeled data, and (c) the comparison of both in spectral cuts.

are nearly symmetric and can be approximated by fitting a Gaussian function (red line). The peak energy and full width at half maximum (FWHM) of the SQW and SML samples are 1.257 eV (5.9 meV) and 1.244 eV (8.1 meV), respectively. The emission of the SML:Sb samples differs significantly from the former in both linewidth and symmetry. The emission is almost 10-fold broadened as compared to the SQW and shows a steep slope at its blue wing and a slow tailing at the red side. The luminescence appears to be well described by a sum of two Gaussian functions, centered at 1.215 eV and 1.176 eV with FWHM of 79.6 meV and 28.2 meV, respectively, separated by 41 meV. This particular shape may be an indication of a bimodal distribution of exciton states in the SML:Sb sample.

Further information about the energetic structure can be gathered from the temperature-dependent luminescence of the SML:Sb sample, as plotted in Fig. 2 (a). The depth of potential traps can be determined by analyzing the activation energy, obtained from temperature dependence of the total luminescence intensity. In Fig. 2 (b) we fit the spectrally integrated luminescence I with a thermally activated quenching model [28] using a scaling parameter C:

$$I(T) = \frac{I(0\ K)}{1 + C \cdot \exp(-E_A/k \cdot T)}, \qquad (1)$$

For the calculation we consider data from 60 K up to room temperature. At lower temperature, the integrated emission shows a dip caused by the charge carrier transfer between strongly and weakly localized states at lower lattice temperature [14], [29]. We obtain an activation energy of E_A = 45 meV, which is very close to the 41 meV energy separation between the two emission peaks indicated in Fig. 1 (f).

The temporal evolution of the photoluminescence spectra after optical excitation are shown in Fig.3 (a). We observe an asymmetric decay on a ns-time scale with slightly longer time constants for the red wing of the spectrum as compared to the blue wing. This is a common observation for SML structures, and stems from the scattering of carriers between localization centers [11], as opposed to pure capture from a reservoir for QDs, for which an even decay across all wavelengths is expected. Interestingly, the PL recorded from the SML:Sb sample shows a combination of both characteristic features. While on the blue side we observe an increasingly fast decay indicating scattering channels in excess of radiative recombination, on the red side the decay is nearly homogeneous. This is one more strong indication for the presence of two distinct subensembles within the SML:Sb sample.

For quantification of our results and to elucidate the electronic structure, we developed a microscopically motivated rate equation model extending our previous work on pure InAs SML QDs [11]. Based on the previous experimental observations of low-temperature photoluminescence we propose an electronic structure of the SML:Sb QDs that consists of three different types of charge-carrier states. 1. The three-dimensional states of the bulk host material surrounding the SML layer from which the charge carriers scatter into the SML states. 2. The weakly localized and laterally extended SML states, which allow for an ultrafast diffusive coupling between the In-rich agglomeration. 3. Localized states due to Sb inclusions within the SML layers, which can capture charge carriers from the surrounding SML states. Both the extended and localized SML states are inhomogeneously broadened, due to the random nature of the In and Sb incorporation, with different widths, $\Delta E_{\mathrm{SML}}^{\mathrm{inhom}}$, $\Delta E_{\mathrm{Sb}}^{\mathrm{inhom}}$, and shape of their distribution. We fit the individual shape of their densities of states to match the experimental photoluminescence data. As the input information is obtained from luminescence data, the DOS has to be considered as an effective exciton DOS. A sketch of the relative contributions of the different material subsystems to the total DOS is shown in Fig. 4, where we refer to "SML" for the weakly localized states and "Sb" to the Sb inclusions. Note that during growth the Sb adatoms tend to

1077-260X (c) 2019 IEEE. Personal use is permitted, but republication/redistribution requires IEEE permission. See http://www.ieee.org/publications_standards/publications/rights/index.html for more information.

This article has been accepted for publication in a future issue of this journal, but has not been fully edited. Content may change prior to final publication. Citation information: DOI 10.1109/JSTQE.2019.2919763, IEEE Journal of Selected Topics in Quantum Electronics

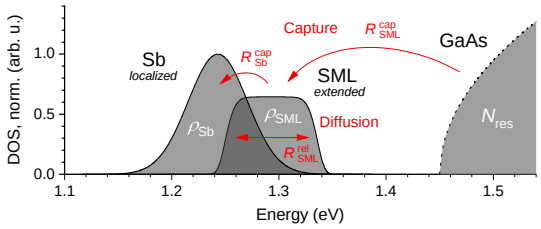


Fig. 4. Modeled effective exciton density of states for the SML:Sb material system. The model considers three charge-carrier states and their interactions: the bulk host material GaAs (not to scale), the lateral extended SML states and the localized Sb states.

cluster and concentrate at the In-rich islands [14], where they increase the hole confinement due to the typical type-II band alignment of bulk InSb/GaSb heterostructures [30].

We consider different types of charge-carrier interactions within and between the different kinds of states. Charge carriers from the bulk states can be captured into the SML states with an effective capture rate that depends on the bulk charge carrier density and thus on the amount of optically created excitons. The weak localization introduces a coupling between the SML states, leading to the ultrafast lateral scattering between them. With these scattering mechanisms the charge carrier dynamics in SML materials can be accurately described [11]. Additionally, we assume localized states introduced by the Sb incorporation energetically below the SML states. Charge carriers from the SMLs can be trapped in the Sb states. Collecting these processes, we are able to write down coupled rate equations for the bulk reservoir charge carrier density N_{res}, the occupation probability of the SML states, $\rho_{\mathrm{SML}}(E)$, and the localized Sb states $\rho_{\mathrm{Sb}}(E)$, both depending on the energy E:

$$\frac{\mathrm{d}}{\mathrm{d}t}N_{\mathrm{res}} = J - \frac{N_{\mathrm{res}}}{\tau_{\mathrm{res}}} - \int \frac{\mathcal{D}_{\mathrm{SML}}(E)}{h_{\mathrm{res}}}\widetilde{R}^{\mathrm{cap}}_{\mathrm{SML}}(E)\mathrm{d}E \tag{2}$$

$$\frac{\mathrm{d}}{\mathrm{d}t}\rho_{\mathrm{SML}}(E) = -\frac{\rho_{\mathrm{SML}}(E)}{\tau_{\mathrm{SML}}} + \widetilde{R}^{\mathrm{cap}}_{\mathrm{SML}}(E) + \widetilde{R}^{\mathrm{rel}}_{\mathrm{SML}}(E) - \int \frac{\mathcal{D}_{\mathrm{Sb}}(E')}{N_{\mathrm{SML}}}\widetilde{R}^{cap}_{\mathrm{Sb}}(E,E')\mathrm{d}E' \tag{3}$$

$$\frac{\mathrm{d}}{\mathrm{d}t}\rho_{\mathrm{Sb}}(E) = -\frac{\rho_{\mathrm{Sb}}(E)}{\tau_{\mathrm{Sb}}} + \int \frac{\mathcal{D}_{\mathrm{SML}}(\tilde{E})}{N_{\mathrm{SML}}}\widetilde{R}^{cap}_{\mathrm{Sb}}(\tilde{E},E)\mathrm{d}\tilde{E}\,. \tag{4}$$

We include the electrical pump current density, J, characteristic charge carrier loss rates, τ_{res}, τ_{SML}, τ_{Sb} in the respective states, and charge carrier scattering processes:

$$\widetilde{R}^{\mathrm{cap}}_{\mathrm{SML}}(E) = R^{\mathrm{cap}}_{\mathrm{SML}}(J)\left[F(E,\mu,T) - \rho^{\mathrm{SML}}(E)\right] \tag{5}$$

$$\widetilde{R}^{\mathrm{rel}}_{\mathrm{SML}}(E) = R^{\mathrm{rel}}_{\mathrm{SML}}\int \frac{\mathcal{D}_{\mathrm{SML}}(\tilde{E})}{N_{\mathrm{SML}}}\Big\{[1-\rho_{\mathrm{SML}}(E)]\rho_{\mathrm{SML}}(\tilde{E}) - \rho_{\mathrm{SML}}(E)[1-\rho_{\mathrm{SML}}(\tilde{E})]\exp\left(\tfrac{E-\tilde{E}}{k_BT}\right)\Big\}\mathrm{d}\tilde{E} \tag{6}$$

$$\widetilde{R}^{\mathrm{cap}}_{\mathrm{Sb}}(E,E') = \Theta(E-E')R^{\mathrm{cap}}_{\mathrm{Sb}}\Big\{[1-\rho_{\mathrm{Sb}}(E')]\rho_{\mathrm{SML}}(E) - \rho_{\mathrm{Sb}}(E')[1-\rho_{\mathrm{SML}}(E)]\exp\left(\tfrac{E'-E}{k_BT}\right)\Big\}\,. \tag{7}$$

Here, $\widetilde{R}^{\mathrm{cap}}_{\mathrm{SML}}(E)$ describes the capture rate of bulk carriers into the SML state at energy E, $\widetilde{R}^{\mathrm{rel}}_{\mathrm{SML}}(E)$ is the diffusive scattering into the SML state at E from all other SML states, and $\widetilde{R}^{\mathrm{cap}}_{\mathrm{Sb}}(E,E')$ denotes the capture of carriers from the SML state at energy E into the localized Sb state at energy E'. $F(E,\mu,T)$ is the Fermi function at energy E and temperature T. The quasi-Fermi level μ in the bulk reservoir is calculated dynamically from the bulk carrier density N_{res} using the effective physical extension h_{res} of the reservoir perpendicular to the active layer. We denote the two-dimensional density of states in the SML and Sb states by $\mathcal{D}_{\mathrm{SML}}(E)$ and $\mathcal{D}_{\mathrm{Sb}}(E)$, respectively. $N_{\mathrm{SML}} = \int \mathcal{D}_{\mathrm{SML}}(E)\mathrm{d}E$ and $N_{\mathrm{Sb}} = \int \mathcal{D}_{\mathrm{Sb}}(E)\mathrm{d}E$ are the integrated two-dimensional areal densities of states. In Eq. (7), Θ is the Heaviside function, i.e., we only allow a capture of charge carriers into Sb states from SML states at a higher energy.

TABLE I
PARAMETERS USED IN THE SIMULATIONS OF THE SML:SB DEVICE.

Quantity	Symbol	Value	
Bulk lifetime	τ_{res}	1 ns	[11]
SML lifetime	τ_{SML}	0.8 ns	[11]
Sb lifetime	τ_{Sb}	0.8 ns	
SML inhom. width	$\Delta E^{\mathrm{inhom}}_{\mathrm{SML}}$	50 meV	
Sb inhom. width	$\Delta E^{\mathrm{inhom}}_{\mathrm{Sb}}$	65 meV	
Bulk reservoir height	h_{res}	350 nm	
SML areal density	N_{SML}	$3.5\cdot10^{11}$ cm^{-2}	[14]
Sb areal density	N_{Sb}	$0.7\cdot10^{11}$ cm^{-2}	
Capture rate into SML	$R^{\mathrm{cap}}_{\mathrm{SML}}(J)$	60 ns$^{-1}\times(J/J_{\mathrm{tr}})^2$	[11]
Diffusive SML scatt. rate	$R^{\mathrm{rel}}_{\mathrm{SML}}$	3.5 ps^{-1}	[11]
Capture rate into Sb	$R^{\mathrm{cap}}_{\mathrm{Sb}}$	1 ps^{-1}	
Internal losses	α_{int}	6.3 cm^{-1}	
Gain coefficient	g	$3\cdot10^{-4}$ eV m^{2}s^{-1}	
Dephasing time	T_2	150 fs	[11]

We proceed by simulating the measured time-resolved photoluminescence spectra from numerical simulations of the rate equations (2)–(4) by analogy to our previous work in Ref. [11]. We extract the photoluminescence spectra, $S(E)$, from the time-resolved charge carrier distributions:

$$S(E) \propto \sum_m \int \rho^m(E')\mathcal{D}_m(E')\mathcal{L}(E'-E)\,\mathrm{d}E', \tag{8}$$

where m iterates over SML and Sb states. We assume a sech-shaped emission lineshape of each optical transition, $\mathcal{L}(E) = \frac{T_2}{\pi\hbar}\,\mathrm{sech}\left(\frac{T_2E}{\hbar}\right)$. To reduce the number of free parameters we used values from literature where available.

The optical excitation was implemented via a Gaussian source term in the carrier reservoir with a temporal length of 230 fs FWHM. Fig. 3 (b) shows the simulated time-resolved photoluminescence spectra after short-pulse excitation. The numerical model accurately reproduces the measured data. From the numerical results, the characteristic tail towards short wavelengths shortly after the excitation can be attributed to the SML states filled from the bulk charge carrier reservoir, which quickly depletes when the charge carriers scatter into the Sb states. The decay of the trapped carriers in these localized states leads to the broad and long-lived emission around 1.21 eV (1025 nm). This broad emission is evidence for a weak coupling between the emitting states, as the carriers

1077-260X (c) 2019 IEEE. Personal use is permitted, but republication/redistribution requires IEEE permission. See http://www.ieee.org/publications_standards/publications/rights/index.html for more information.

This article has been accepted for publication in a future issue of this journal, but has not been fully edited. Content may change prior to final publication. Citation information: DOI 10.1109/JSTQE.2019.2919763, IEEE Journal of Selected Topics in Quantum Electronics

remain trapped without thermalizing. All obtained parameters were listed in Tab. I.

IV. Application to Semiconductor Lasers and Optical Amplifiers

The effective gain bandwidth accompanied by e.g. the external quantum efficiency, lasing threshold, gain recovery time, and amplitude phase coupling represent important key parameters for opto-electronic devices. In the following section, we will analyze the static output performance of SCLs based on a single layer of SML:Sb QDs in comparison to lasers based on a SQW or a single layer of non-alloyed SML QDs as active medium.

The remarkably broad PL emission of the SML:Sb sample in Sec. III is also observed in the electroluminescence (EL) spectra of the respective SCLs as shown in Figs. 5 (a) - (c) for injection currents ranging from 0.25 to 0.95 times their particular lasing threshold J_{th}. At low currents the emission bandwidth accountes for 31 nm (34 meV) to 37 nm (40 meV) and 50 nm (54 meV) for the SQW, SML and SML:Sb lasers, respectively. Dash-dotted lines mark the position of the laser lines appearing above threshold. For the SQW and the SML lasers, the rise in intensity with increasing current leads to only minor spectral shifts, and the lasing line appears at the position of maximum intensity. For the SML:Sb laser, there is an apparent crossover in the dominant contribution to the EL from localized to delocalized states, with lasing starting from the latter. The total blue-shift of the emission maximum from low current to lasing threshold is 34 nm (37 meV), which roughly corresponds to the energy separation of the two distinct exciton states derived in Sec. III.

As in Stranski-Krastanow QD based excited state lasers, the reason for such a behavior can be found in the lower gain owing to the lower DOS in the localized states of low energy [31]. We thus address the lasing states to the extended SML rather than the localized Sb states. This leads to the assumption of ultrafast gain recovery as known for QD excited state lasers [32] by costs of an enhanced threshold current due to the need of state filling. That assumption reflects in the light-current characteristics as shown in Fig. 5 (d). The devices start lasing at 8.9 mA, 8.1 mA, and 43.2 mA for the SQW, SML, and SML:Sb laser, respectively. Further we extract the external quantum efficiency, namely the number of emitted photons per injected electron-hole pair, from the slope of the optical power and the lasing frequency ν: [33]

$$\eta_{\text{ext}} = \frac{2e}{h\nu}\frac{dP_{\text{ext}}}{dI}. \tag{9}$$

All devices show comparable values of 33 % per facet.

Large Material Gain: In SOAs based on pure InAs SML QDs, we found a relatively large modal gain and a narrow gain bandwidth with fast gain recovery [11]. In this study we use the standard Hakki-Paoli method [27] to obtain the net modal gain $\mathcal{G}_{\text{net}}$ and thus the material gain g_{mat} of the lasers. Both parameters are linked via the the mode-confinement factor Γ and the waveguide losses α_{int}:

$$\mathcal{G}_{\text{net}} = \mathcal{G} - \alpha_{\text{int}} = \Gamma g_{\text{mat}} - \alpha_{\text{int}}. \tag{10}$$

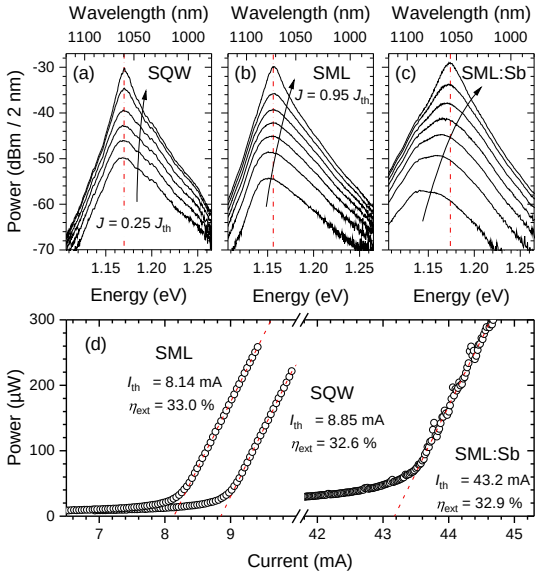


Fig. 5. Room temperature electroluminescence spectra of a (a) SQW, (b) SML and (c) SML:Sb laser for injection currents ranging from 0.25 to 0.95 times the respective threshold current. The dash-dotted lines mark the respective lasing wavelengths. (d) Light-current characteristics of all devices and linear fit to determine the respective threshold current and quantum efficiency.

Using a high resolution optical spectrum analyzer we calculate $\mathcal{G}_{\text{net}}$ from the spectral peak to valley ratio r of the cavity Fabry-Pérot modes below threshold:

$$\mathcal{G}_{\text{net}} = \frac{1}{\ell}\ln\left(\frac{\sqrt{r}-1}{\sqrt{r}+1}\right) - \frac{1}{\ell}\ln(R), \tag{11}$$

with the cavity length ℓ and mirror reflectivity R. Fig. 6 (a) shows the derived gain spectra of SQW, SML and SML:Sb based SCLs with 0.5 mm cavity length and 3 μm ridge width driven at 0.95 times their respective threshold current J_{th}. We find the narrowest and largest gain for the SQW based device and an increasing bandwidth for the SML up to the SML:Sb SCL accompanied by a reduction of the peak gain. The derived parameters are listed in Tab. II.

In Fig. 6 (b) we show the derived gain curves of the SML:Sb laser for different injection currents ranging from $J = 0.25...0.95 \times J_{th}$ as black symbols. The dashed red lines represent fits based on the numerical model of Sec. III [34], calculated according to

$$\mathcal{G}_{\text{net}}(E) = \frac{g}{v_g}\sum_m \int [2\rho^m(E')-1]\mathcal{D}_m(E')\mathcal{L}(E'-E)\mathrm{d}E' - \alpha_{\text{int}} \tag{12}$$

with the group velocity v_g and the gain coefficient g, which implicitly contains the waveguide properties as a fitting parameter (see Tab. I).

The relatively large peak shift of roughly 40 meV (37 nm) from low injection currents up to 0.95 J_{th} is in good agreement to the blue-shifted lasing wavelength from the EL spectra. This further supports our assumption of a bimodal electronic structure containing SML and Sb states and allows us to determine the internal losses α_{int} of the SML:Sb laser to $\alpha_{\text{int}} = 6.3$ cm^{-1}. Due to the identical waveguide structures

1077-260X (c) 2019 IEEE. Personal use is permitted, but republication/redistribution requires IEEE permission. See http://www.ieee.org/publications_standards/publications/rights/index.html for more information.

This article has been accepted for publication in a future issue of this journal, but has not been fully edited. Content may change prior to final publication. Citation information: DOI 10.1109/JSTQE.2019.2919763, IEEE Journal of Selected Topics in Quantum Electronics

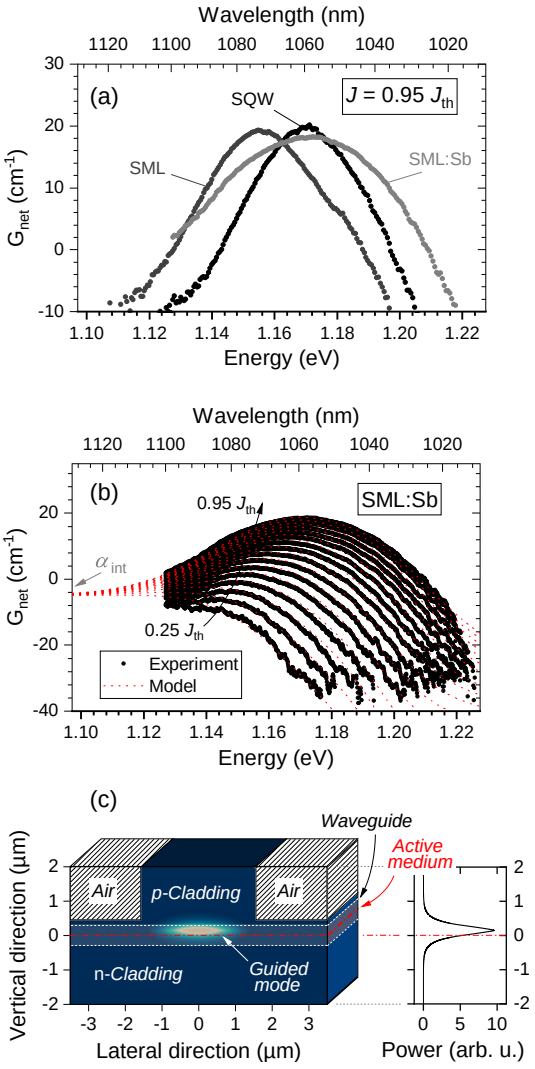


Fig. 6. (a) Measured net modal gain of a SQW, SML and SML:Sb based lasers with a 0.5 mm cavity at 0.95 times their respective threshold current. (b) Measured and modelled gain spectra of the SML:Sb laser for injection currents ranging from 0.25 to 0.95 times the threshold current. (c) Simulation of the electric field distribution within the layer structure for confinement factor calculation.

TABLE II
LASER GAIN AT A DRIVING CURRENT OF 0.95 J_{th}.

Parameter		SQW	SML	SML:Sb
$g_{\mathrm{net,max}}$	/ cm^{-1}	20.2	19.3	18.3
Δg_{3dB}	/ nm	13.7	17.9	28.0
d	/ nm	8.3	5.7	3.5
Γ	/ %	3.8	2.6	1.6
$g_{\mathrm{mat,max}}$	/ cm^{-1}	700	1000	1500

of all devices we assume comparable losses for the SQW and SML SCLs within the error margins of approximately 5 %. The current dependency of $R_{\mathrm{SML}}^{\mathrm{cap}}$ in Tab. I contains the transparency current J_{tr} obtained from single-color pump-probe measurements at the maximum of the gain distribution as a scaling factor.

The material gain g_{mat} is scaled with the confinement factor Γ, which is defined as the ratio of the electric field distribution

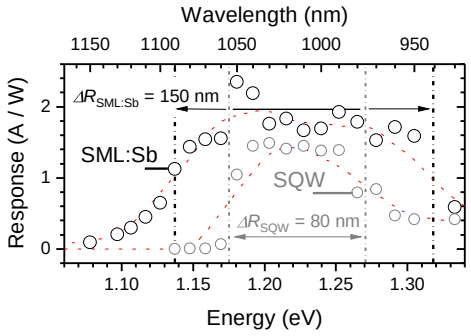


Fig. 7. Spectral response of an SML:Sb SOA in comparison to a SQW SOA at -1 V bias and 10 nm excitation bandwidth. ΔR marks the response bandwidth of both devices.

$E_z^2(x,y)$ within the active medium i to the total electric field distribution: [35]

$$\Gamma = \frac{\int_i E_z^2(x,y)\ dxdy}{\int_{-\infty}^{\infty} E_z^2(x,y)\ dxdy}. \tag{13}$$

We model the transversal electric field distribution from the epitaxial layer structure using a semi-analytical mode-solver [36], which is shown in Fig. 6 (c). Due to the identical waveguide structures, the size of Γ exclusively depends on the respective width of the active medium, sketched as white line in the figure. Due to the growth protocols we assume total material thicknesses of 8.3, 5.7 nm and 3.5 nm for the SQW, SML and SML:Sb layers, respectively. Following Eq. 10 we thus determine the material gain via $g_{\mathrm{mat}} = (\mathcal{G}_{\mathrm{net}} + \alpha_{\mathrm{int}}) \cdot \Gamma^{-1}$ and find increasing values from 700 to 1500 cm^{-1} for the SQW to the SML:Sb sample, as listed in Tab. II. Note that the values of material gain per layer of the dot structures as sketched in Fig. 1 refer to the particular layer forming the active medium rather than to the isolated dots.

Broad Optical Response: The broadened gain spectrum of SML:Sb lasers certainly vanishes in lasing operation, as mode competition will collapse the spectrum to few competing lasing modes. However in case of superluminescence devices or optical amplifiers the full spectrum will be maintained. In the following part we will apply the material into SOAs and analyze the broadband response, gain dynamics and amplitude-phase coupling.

Like the luminescence, the optical response R of SOAs based on a SQW and a single layer of SML:Sb QDs shows the broadband capabilities of the latter. R relates the average induced photocurrent $I(\lambda)$ after external optical excitation with an optical power P_{in} via $I(\lambda) = R(\lambda) \cdot P_{\mathrm{in}}$ and was measured via incoupling of a spectrally tunable optical pulse into the SOA at reverse bias. A brief estimate for the ionizability of optically induced excitons within the active region leads to the assumption that a reverse bias of -1 V already ensures sufficient carrier transport.

As shown in Fig. 7 we find an enhanced response bandwidth of roughly 150 nm (180 meV) for the SML:Sb SOA as compared to 80 nm (95 meV) for the SQW SOA. This is due to the two-fold DOS of the SML:Sb QD material system,

1077-260X (c) 2019 IEEE. Personal use is permitted, but republication/redistribution requires IEEE permission. See http://www.ieee.org/publications_standards/publications/rights/index.html for more information.

This article has been accepted for publication in a future issue of this journal, but has not been fully edited. Content may change prior to final publication. Citation information: DOI 10.1109/JSTQE.2019.2919763, IEEE Journal of Selected Topics in Quantum Electronics

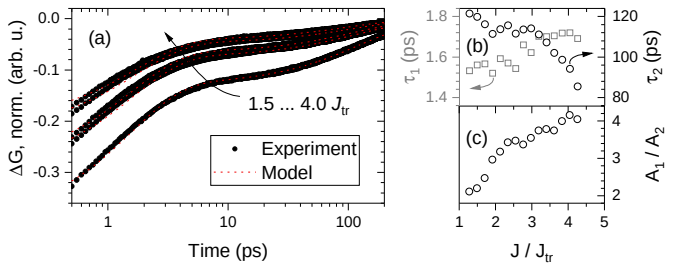


Fig. 8. (a) Gain recovery of an amplifying SML:Sb SOA obtained from heterodyne-detected pump-probe spectroscopy in resonance to the spectral gain peak at 1060 nm, which is mainly formed by delocalized SML states. Dashed lines mark the results of a biexponential fit. The extracted time constants in (b) are referred to processes of thermalization included in τ_1 and state filling on the time scale of τ_2. The amplitude ratio of both time constants is plotted in (c).

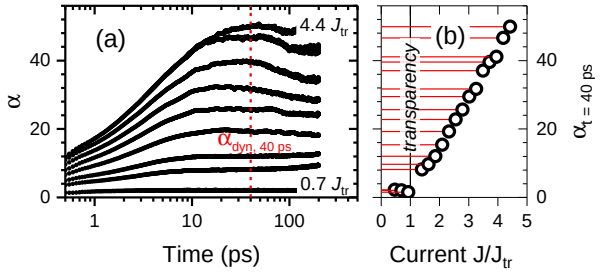


Fig. 9. (a) Temporal development and (b) quasi-steady state value of the α parameter obtained from Eq. 15 after measuring the gain and phase change within the SML:Sb SOA.

which is additionally verified in the peak of the response around 1050 nm. The enlarged bandwidth of the response in comparison to the SQW is a promising feature for possible applications as, e.g., semiconductor photodetectors.

Ultrafast Gain Dynamics: An important figure of merit for the potential performance of SOAs is, apart from the gain magnitude, the gain recovery rate, as it limits the modulation speed of the device. The dynamics can be extracted from pump-probe experiments, in which a probe pulse with variable time delay samples the return to equilibrium of the device after perturbation with a pump pulse. We performed a series of single-color pump-probe experiments on an SML:Sb SOA. Note that the angled and anti-reflection coated facets of an SOA ensure a single-transition pulse modulation.

Figs. 8 (a) and (b) show the measured gain recovery traces for different injection currents (dots) and corresponding biexponential fits (dashed lines) to obtain the gain recovery time constants. The differential change in the measured signal is negative as the probe pulse samples a system in which carriers were depleted by the pump pulse. The transparency current was determined as the current at which the probe pulse does not experience a change in its amplitude. In Fig. 8 (b) we plot the extracted time constants from the fit, where we attribute the fast recovery τ_1 to a fast inter-dot capture process and the slow recovery τ_2 to the state-refilling from the carrier reservoir. Remarkably, both time constants are faster than the time constants observed for pure InAs SML QDs. [10]. This may originate from the particular energy level structure, in which the optically active levels form an intermediate state comparable to the conditions in excited state lasers, which also show a remarkably fast gain recovery [32]. The amplitude ratio in Fig. 8 (c) shows an increasing dominance of the faster recovery process τ_1 with increasing injection current above threshold.

Large Amplitude-Phase Coupling: The heterodyne detected pump-probe experiment measures both amplitude and phase changes of the probe pulse. As the phase change is directly related to refractive index variations induced by the pump pulse, we can extract the α parameter quantifying amplitude-phase coupling. In a previous experiment, we demonstrated a large interdependence of the optical gain g and refractive index n in SOAs based on pure InAs SML QDs [11], [12]. The classical definition of the α parameter relates the carrier population N, the optical gain g and refractive index n at the wavelength λ via [37]

$$\alpha = -\frac{4\pi}{\lambda} \cdot \frac{\mathrm{d}n/\mathrm{d}N}{\mathrm{d}g/\mathrm{d}N}. \tag{14}$$

This expression can be recast as

$$\alpha_{\mathrm{dyn}}(t) = -\frac{20}{\ln 10} \cdot \frac{\Delta\Phi(t)}{\Delta G(t)}, \tag{15}$$

using the differential changes in amplitude $\Delta G(t)$ and phase $\Delta\Phi(t)$ recorded in our pump-probe experiment [38]. It is well known that different experimental approaches are prone to yield differing numbers for the value of α [39], and care must be taken when comparing values for the parameter obtained under different conditions. We thus labeled the expression above by the index dyn to highlight that it was obtained from a dynamical experiment on the system under nonequilibrium conditions. This is also contained in the marked time dependence of the value of α_{dyn} reflecting the spreading of the perturbation in space and energy from the exciton interacting resonantly with the pump light. In that dynamical process the energetically blue-shifted carrier reservoir replenishes the gain via down-scattering and simultaneously induces a phase response due to the spectrally biased carrier distribution.

The dynamic alpha parameter of the SML:Sb SOA is shown in Fig. 9 (a) and shows a comparable temporal development to observations for pure InAs SML QDs based SOAs [12]. At small delay times and low currents we obtain a single-digit value for α_{dyn}, followed by a rise to very high values of up to 50 on the timescale of 10 ps. This rise time is much faster than for pure InAs SML QDs, though in some cases in particular for large currents there is a small overshoot with the final equilibrium value being reached at about 40 ps. In practical applications, e.g. optical telecommunications, such devices are not driven in continuous mode but modulated with up to a double-digit GHz rate. Thus the technically relevant α_{dyn} is then given by its saturation value at long delay times.

These quasi-steady state values are plotted in Fig. 9 (b) versus injection current. We find a monotonic growth of α_{dyn} from values close to unity at transparency up to values above 40 when operating the device at the fourfold transparency

1077-260X (c) 2019 IEEE. Personal use is permitted, but republication/redistribution requires IEEE permission. See http://www.ieee.org/publications_standards/publications/rights/index.html for more information.

This article has been accepted for publication in a future issue of this journal, but has not been fully edited. Content may change prior to final publication. Citation information: DOI 10.1109/JSTQE.2019.2919763, IEEE Journal of Selected Topics in Quantum Electronics

current. The high value of α_{dyn} signifies that devices based on SML:Sb QDs will display large optical nonlinearities. Furthermore, assuming a constant dependence for $n(N)$ in Eq. 14, the linear increase of α_{dyn} indicates a reciprocal dependency $g(N) \propto N^{-1}$, which is the case for, e.g., free carrier absorption [40], [41]. It needs to be stated that the dynamical α parameter is by no means considered as constant, as carrier thermalization and recombination are nonlinear processes with different contributions to gain and refractive index modulation. Nevertheless for constant driving conditions α becomes constant and can gain higher values for the SML:Sb material system.

V. Conclusions

To conclude, we investigated the luminescence properties of submonolayer grown InGa(Sb)As quantum dots emitting around 1060 nm with respect to their excitonic energy structure and dynamics. In a comparative study with a single quantum well and a submonolayer grown InGa(Sb)As quantum dot sample emitting in the same wavelength range we find a 10-fold linewidth broadening due to a Sb-induced bimodal state distribution. The photoluminescence obtained from the samples at low temperature showed a decay on a ns timescale. Based on a microscopically motivated rate equation model, the data could be decomposed into contributions from isolated as well as from laterally coupled states. The model yields an effective density of states with a 0D confined state at lower energy and a higher-energy extended state. The latter has been found already in pure submonolayer grown InGaAs quantum dots [11]. The application of SML:Sb QDs for semiconductor lasers revealed a large material gain of 1500 cm^{-1}, exceeding the value for the quantum well and pure submonolayer reference devices. This is of particular interest due to the broadband nature of the SML:Sb emission, which may be used to replace a stack of chirped QWs by a single active layer. In optical amplifiers based on SML:Sb QDs we find an ultrafast gain recovery and very large spectral bandwidth. These are favorable properties for applications in, e.g., optical networks. As to InAs SML QDs, the amplitude-phase coupling is large, suggesting an application as frequency converter, e.g. by cross phase modulation, rather than as linear amplifier. While the localized lower-energy states play little role for lasing and amplification action, the full bandwidth of electronic states contributes if SML:Sb QDs are applied in photo-detectors, increasing the usable bandwidth for detection even beyond the bandwidth for emission.

Acknowledgments We acknowledge Jan-Hindrik Schulze for his support at sample growth. This research was funded by Deutsche Forschungsgemeinschaft via SFB 787, GRK 1558 and AC 290-2/1.

References

[1] A. M. Fox, "Optoelectronics in quantum well structures," *Contemp. Phys.*, vol. 37, no. 2, pp. 111–125, 1996.

[2] D. Bimberg, N. Kirstaedter, N. N. Ledentsov, Z. I. Alferov, P. S. Kop, and V. M. Ustinov, "InGaAs – GaAs Quantum-Dot Lasers," *IEEE J. Sel. Top. Quantum Electron.*, vol. 3, no. 2, pp. 196–205, 1997.

[3] W. W. Chow, M. Lorke, and F. Jahnke, "Will quantum dots replace quantum wells as the active medium of choice in future semiconductor lasers?," *IEEE J. Sel. Top. Quantum Electron.*, vol. 17, no. 5, pp. 1349–1355, 2011.

[4] D. Bimberg and U. W. Pohl, "Quantum dots: promises and accomplishments," *Mater. Today*, vol. 14, pp. 388–397, sep 2011.

[5] M. Kolarczik, N. Owschimikow, B. Herzog, F. Buchholz, Y. Kaptan, and U. Woggon, "Exciton dynamics probe the energy structure of a quantum dot-in-a-well system: The role of Coulomb attraction and dimensionality," *Phys. Rev. B*, vol. 91, p. 235310, jun 2015.

[6] S. S. Mikhrin, A. E. Zhukov, A. R. Kovsh, N. A. Maleev, I. S. Tarasov, D. A. Bedarev, B. V. Volovik, M. V. Maximov, and Z. I. Alferov, "0 . 94 μ m diode lasers based on Stranski – Krastanow and sub-monolayer quantum dots," *Semicond. Sci. Technol.*, vol. 15, pp. 1061–1064, 2000.

[7] T. D. Germann, A. Strittmatter, J. Pohl, U. W. Pohl, D. Bimberg, J. Rautiainen, M. Guina, and O. G. Okhotnikov, "High-power semiconductor disk laser based on InAs/GaAs submonolayer quantum dots," *Appl. Phys. Lett.*, vol. 92, no. 10, p. 101123, 2008.

[8] S. Upadhyay, A. Mandal, N. B. V. Subrahmanyam, P. Singh, P. Shete, B. Tongbram, and S. Chakrabarti, "Effects of high-energy proton implantation on the luminescence properties of InAs submonolayer quantum dots," *J. Lumin.*, vol. 171, pp. 27–32, 2016.

[9] D. Das, H. Ghadi, S. Sengupta, A. Ahmad, A. Manohar, and S. Chakrabarti, "Optimization of the number of stacks in the submonolayer quantum dot heterostructure for infrared photodetectors," *IEEE Trans. Nanotechnol.*, vol. 15, no. 2, pp. 214–219, 2016.

[10] B. Herzog, N. Owschimikow, J.-H. Schulze, R. Rosales, Y. Kaptan, M. Kolarczik, T. Switaiski, A. Strittmatter, D. Bimberg, U. W. Pohl, and U. Woggon, "Fast gain and phase recovery of semiconductor optical amplifiers based on submonolayer quantum dots," *Appl. Phys. Lett.*, vol. 107, no. 201102, pp. 1–4, 2015.

[11] B. Lingnau, K. Lüdge, B. Herzog, M. Kolarczik, Y. Kaptan, U. Woggon, and N. Owschimikow, "Ultrafast gain recovery and large nonlinear optical response in submonolayer quantum dots," *Phys. Rev. B*, vol. 94, no. 1, p. 014305, 2016.

[12] B. Herzog, B. Lingnau, M. Kolarczik, Y. Kaptan, D. Bimberg, A. Maaßdorf, U. W. Pohl, R. Rosales, J.-H. Schulze, A. Strittmatter, M. Weyers, U. Woggon, K. Lüdge, and N. Owschimikow, "Strong amplitude-phase coupling in submonolayer quantum dots," *Appl. Phys. Lett.*, vol. 109, no. 20, p. 201102, 2016.

[13] A. Lenz, H. Eisele, J. Becker, L. Ivanova, E. Lenz, F. Luckert, K. Pötschke, A. Strittmatter, U. W. Pohl, D. Bimberg, and M. Dähne, "Atomic Structure of Buried InAs Sub-Monolayer Depositions in GaAs," *Appl. Phys. Express*, vol. 3, p. 105602, oct 2010.

[14] D. Quandt, J.-H. Schulze, A. Schliwa, Z. Diemer, C. Prohl, A. Lenz, H. Eisele, A. Strittmatter, U. W. Pohl, M. Gschrey, S. Rodt, S. Reitzenstein, D. Bimberg, M. Lehmann, and M. Weyland, "Strong charge-carrier localization in InAs/GaAs submonolayer stacks prepared by Sb-assisted metalorganic vapor-phase epitaxy," *Phys. Rev. B*, vol. 91, no. 23, p. 235418, 2015.

[15] C. G. E. Alfieri, D. Waldburger, J. Nürnberg, M. Golling, L. Jaurigue, K. Lüdge, and U. Keller, "Mode-locking Instabilities for High-Gain Semiconductor Disk Lasers Based on Active Submonolayer Quantum Dots," *Phys. Rev. Appl.*, vol. 10, no. 4, p. 044015, 2018.

[16] J. G. Fujimoto, "Optical coherence tomography for ultrahigh resolution in vivo imaging," *Nat. Biotechnol.*, vol. 21, no. 11, pp. 1361–1367, 2003.

[17] S. Marschall, C. Pedersen, and P. E. Andersen, "Investigation of the impact of water absorption on retinal OCT imaging in the 1060 nm range," *Biomed. Opt. Express*, vol. 3, no. 7, p. 1620, 2012.

[18] G. Matthäus, T. Schreiber, J. Limpert, S. Nolte, G. Torosyan, R. Beigang, S. Riehemann, G. Notni, and A. Tünnermann, "Surface-emitted THz generation using a compact ultrashort pulse fiber amplifier at 1060 nm," *Opt. Commun.*, vol. 261, no. 1, pp. 114–117, 2006.

[19] D. Quandt, J. Bläsing, and A. Strittmatter, "Analysis of InAsSb/GaAs submonolayer stacks," *J. Cryst. Growth*, vol. 494, pp. 1–7, 2018.

[20] N. N. Ledentsov, D. Bimberg, F. Hopfer, A. Mutig, V. A. Shchukin, A. V. Savel'Ev, G. Fiol, E. Stock, H. Eisele, M. Dähne, D. Gerthsen, U. Fischer, D. Litvinov, A. Rosenauer, S. S. Mikhrin, A. R. Kovsh, N. D. Zakharov, and P. Werner, "Submonolayer quantum dots for high speed surface emitting lasers," *Nanoscale Res. Lett.*, vol. 2, no. 9, pp. 417–429, 2007.

[21] L. Yu, D. Jung, S. Law, J. Shen, J. J. Cha, M. L. Lee, and D. Wasserman, "Controlling quantum dot energies using submonolayer bandstructure engineering," *Appl. Phys. Lett.*, vol. 105, no. 8, pp. 0811030–0811035, 2014.

[22] A. Manohar, S. Sengupta, H. Ghadi, and S. Chakrabarti, "A detailed study of the effects of rapid thermal annealing on the luminescence

1077-260X (c) 2019 IEEE. Personal use is permitted, but republication/redistribution requires IEEE permission. See http://www.ieee.org/publications_standards/publications/rights/index.html for more information.

This article has been accepted for publication in a future issue of this journal, but has not been fully edited. Content may change prior to final publication. Citation information: DOI 10.1109/JSTQE.2019.2919763, IEEE Journal of Selected Topics in Quantum Electronics

properties of InAs sub-monolayer quantum dots," *J. Lumin.*, vol. 158, pp. 149–152, 2015.
[23] R. Kumar, Y. Maidaniuk, A. Kuchuk, S. K. Saha, P. K. Ghosh, Y. I. Mazur, E. Morgan, G. J. Salamo, R. Kumar, Y. Maidaniuk, A. Kuchuk, S. K. Saha, P. K. Ghosh, Y. I. Mazur, M. E. Ware, and G. J. Salamo, "Excitation intensity and thickness dependent emission mechanism from an ultrathin InAs layer in GaAs matrix," *J. Appl. Phys.*, vol. 124, no. 23, p. 235303, 2018.
[24] S. Harrison, M. P. Young, P. D. Hodgson, R. J. Young, M. Hayne, L. Danos, A. Schliwa, A. Strittmatter, A. Lenz, H. Eisele, U. W. Pohl, and D. Bimberg, "Heterodimensional charge-carrier confinement in stacked submonolayer InAs in GaAs," *Phys. Rev. B*, vol. 93, no. 8, p. 085302, 2016.
[25] J. O. Kim, Z. Ku, A. Urbas, and S. J. Lee, "Investigation of the shape of submonolayer quantum dots using a polarization-dependent photocurrent," *Semicond. Sci. Technol.*, vol. 30, no. 11, p. 115005, 2015.
[26] D. Guimard, M. Nishioka, S. Tsukamoto, and Y. Arakawa, "Effect of antimony on the density of InAs/Sb:GaAs(1 0 0) quantum dots grown by metalorganic chemical-vapor deposition," *J. Cryst. Growth*, vol. 298, no. SPEC. ISS, pp. 548–552, 2007.
[27] B. W. Hakki and T. L. Paoli, "Gain spectra in GaAs double-heterostructure injection lasers," *J. Appl. Phys.*, vol. 46, no. 3, pp. 1299–1306, 1975.
[28] E. C. Le Ru, J. Fack, and R. Murray, "Temperature and excitation density dependence of the photoluminescence from annealed InAs/GaAs quantum dots," *Phys. Rev. B*, vol. 67, no. 24, pp. 1–12, 2003.
[29] Q. Li, S. J. Xu, M. H. Xie, and S. Y. Tong, "Origin of the 'S-shaped' temperature dependence of luminescent peaks from semiconductors," *J. Phys. Condens. Matter*, vol. 17, no. 30, pp. 4853–4858, 2005.
[30] Y. I. Mazur, V. G. Dorogan, G. J. Salamo, G. G. Tarasov, B. L. Liang, C. J. Reyner, K. Nunna, and D. L. Huffaker, "Coexistence of type-I and type-II band alignments in antimony-incorporated InAsSb quantum dot nanostructures Yu.," *Appl. Phys. Lett.*, vol. 100, p. 033102, 2012.
[31] Y. Kaptan, H. Schmeckebier, B. Herzog, D. Arsenijević, M. Kolarczik, V. Mikhelashvili, N. Owschimikow, G. Eisenstein, D. Bimberg, and U. Woggon, "Gain dynamics of quantum dot devices for dual-state operation," *Appl. Phys. Lett.*, vol. 104, p. 261108, jun 2014.
[32] Y. Kaptan, A. Röhm, B. Herzog, B. Lingnau, H. Schmeckebier, D. Arsenijević, V. Mikhelashvili, O. Schöps, M. Kolarczik, G. Eisenstein, D. Bimberg, U. Woggon, N. Owschimikow, and K. Lüdge, "Stability of quantum-dot excited-state laser emission under simultaneous ground-state perturbation," *Appl. Phys. Lett.*, vol. 105, no. 19, p. 191105, 2014.
[33] P. Smowton and P. Blood, "The differential efficiency of quantum-well lasers," *IEEE J. Sel. Top. Quantum Electron.*, vol. 3, pp. 491–498, apr 1997.
[34] B. Lingnau, K. Lüdge, W. W. Chow, and E. Schöll, "Failure of the α factor in describing dynamical instabilities and chaos in quantum-dot lasers," *Phys. Rev. E*, vol. 86, no. 6, pp. 1–5, 2012.
[35] T. D. Visser, H. Blok, B. Demeulenaere, and D. Lenstra, "Confinement factors and gain in optical amplifiers," *IEEE J. Quantum Electron.*, vol. 33, no. 10, pp. 1763–1766, 1997.
[36] A. Ivanova, R. Stoffer, and M. Hammer, "A variational mode solver for optical waveguides based on quasi-analytical vectorial slab mode expansion," *ArXiv e-prints*, vol. 1307.1315, pp. 1–19, 2013.
[37] C. H. Henry, "Theory of the linewidth of semiconductor lasers," *Quantum Electron. IEEE J.*, vol. 18, no. 2, pp. 259–264, 1982.
[38] S. Schneider, P. Borri, W. Langbein, U. Woggon, R. Sellin, D. Ouyang, and D. Bimberg, "Linewidth enhancement factor in InGaAs quantum dot amplifiers," *IEEE J. Quantum Electron.*, vol. 40, no. 10, pp. 1423–1429, 2004.
[39] M. Osinski and J. Buus, "Linewidth broadening factor in semiconductor lasers–An overview," *IEEE J. Quantum Electron.*, vol. 23, no. 1, pp. 9–29, 1987.
[40] N. S. N. Storkfelt, B. M. B. Mikkelsen, D. O. D. Olesen, M. Y. M. Yamaguchi, and K. S. K. Stubkjaer, "Measurement of carrier lifetime and linewidth enhancement factor for 1.5- mu m ridge-waveguide laser amplifier," *IEEE Photonics Technol. Lett.*, vol. 3, no. 7, pp. 632–634, 1991.
[41] J. Stohs, D. J. Bessert, D. J. Gallant, and S. R. J. Brueck, "Gain, refractive index change, and linewidth enhancement factor in broad-area GaAs and InGaAs quantum-well lasers," *IEEE J. Quantum Electron.*, vol. 37, no. 11, pp. 1449–1459, 2001.



Bastian Herzog received his M.Sc. degree in physics from the TU Berlin in 2014, where he is working as a Ph.D. student at the institute of optics and atomic physics. His research includes ultrafast spectroscopy on novel semiconductor gain materials for opto-electronic applications.

Benjamin Lingnau Benjamin Lingnau obtained his doctoral degree in physics from the Institute of Theoretical Physics at TU Berlin in 2015 on the nonlinear dynamics of semiconductor quantum-dot material. He is currently with the University College Cork and Tyndall National Institute, Cork, Ireland. His research interests include nonlinear laser dynamics, modeling of the optical and dynamic properties of novel semiconductor active materials, and their applications in opto-electronic devices.



Mirco Kolarczik received his Diploma and Dr. rer. nat. degree in physics from the TU Berlin, Germany in 2012 and 2019, respectively, where he is currently working as a postdoctoral researcher. His research interests include the spectroscopic analysis of complex semiconductor systems of mixed dimensionality and multidimensional coherent spectroscopy.

Sophia Helmrich received her M.Sc. degree in physics from the University of Leipzig, Germany in 2016. She is currently working at the TU Berlin in the field of spectroscopy on mono- and bilayer transition metal dichalcogenides.

Alexander W. Achtstein Alexander W. Achtstein received a Ph.D. in physics from the TU Berlin after studying Physics at LMU Munich and University of Augsburg. After a postdoc at TU Berlin and a two year postdoc at Delft University of Technology he returned to TU Berlin working as a senior scientist in the field of linear and nonlinear optical properties of nano structures, with a focus on colloidal 2D semiconductors.

Kevin Thommes received the M.Sc. degree in physics from TU Berlin in 2018.

Fuad Alhussein received the M.Sc. degree in physics from TU Berlin in 2018.

David Quandt received the Dr. rer. nat. in physics from the TU Berlin in 2018.

André Strittmatter received the Diploma degree in physics, the Dr.rer.nat. degree in natural sciences, and the Habilitation degree in experimental physics from the TU Berlin, Germany, in 1996, 2002, and 2012, respectively. He joined the Institute of Experimental Physics, University of Magdeburg, Germany, in 2014, as an Interim Head of the Group for Semiconductor Epitaxy, where he is involved in nitride-based devices.

1077-260X (c) 2019 IEEE. Personal use is permitted, but republication/redistribution requires IEEE permission. See http://www.ieee.org/publications_standards/publications/rights/index.html for more information.

This article has been accepted for publication in a future issue of this journal, but has not been fully edited. Content may change prior to final publication. Citation information: DOI 10.1109/JSTQE.2019.2919763, IEEE Journal of Selected Topics in Quantum Electronics



Udo W. Pohl Udo W. Pohl studied physics in Aachen and Berlin, Germany, and received his Ph.D. degree in 1988 from the Technical University of Berlin, where he is currently principal investigator in the Institute of Solid State Physics. He is member of the German Physical Society, participated in committees of international conferences, and has given lectures on semiconductor physics and epitaxy since the early 1990ies. In 2009, he was appointed as an Adjunct Professor of Physics at Technical University of Berlin. He has authored over 200 journal articles and conference papers, the monographs "Epitaxy of Semiconductors" and - together with K.W. Böer - "Semiconductor Physics", ten book contributions, and several patents. His current research interests include physics and epitaxy of semiconductor nanostructures and devices.

Olaf Brox Olaf Brox received the M.Sc. degree in physics from the University of Essex, U.K., in 1995 and the Dipl.-Phys. degree from the University of Jena, Germany, in 1997. After his Ph.D. degree at Heinrich-Hertz-Institute and TU Berlin, Germany, in 2005 he joined the Ferdinand-Braun-Institut, Leibniz-Institut für Höchstfrequenztechnik, Berlin, Germany where he is responsible for the development and the fabrication of highly brilliant diode lasers.

Markus Weyers Markus Weyers received the Diploma degree in physics and the Dr. rer. nat. degree from RWTH Aachen, Aachen, Germany, in 1986 and 1990. From August 1990 to March 1992, he was with the NTT Basic Research Labs, Musashino, Japan. Since April 1992, he has been the Head of the Materials Technology Department at Ferdinand-Braun-Institut, Leibniz-Institut für Höchstfrequenztechnik, Berlin, Germany. Since June 2014, he has been an Adjunct Professor with the TU Berlin, where he teaches Applied Physics. His research interests include MOVPE growth of GaAs- and GaN-based laser structures, GaN-based lasers, LEDs and transistor structures and HVPE for GaN and AlGaN substrates. He has authored and coauthored around 500 scientific papers and book chapters on growth studies as well as device growth in MOVPE, MOMBE, and HVPE. He is associate editor for IEEE Photonics Technology Letters and for Journal of Crystal Growth. In 1999, he founded the epiwafer foundry Three-Five Epitaxial Services AG which he headed until the end of 2008. In 1999, he also cofounded LayTec GmbH (now LayTec AG), a producer of in-situ metrology tools for MOVPE.

Ulrike Woggon received the Diploma degree in physics and the Dr. rer. nat. degree from the HU Berlin, Germany, in 1982 and 1985 and the Habilitation degree from University of Kaiserslautern in 1995. From 1997 to 2008 she worked as professor for experimental physics at the TU Dortmund. Since 2008 she is a professor for Nonlinear Optics at the physics deparment of TU Berlin. Her main research interest is the optical spectroscopy of low dimensional semiconductor structures.

Kathy Lüdge was born in Berlin, Germany, in 1976. Since 2016 she is a professor for Theoretical Physics at the TU Berlin and currently on a one year Humboldt Fellowship in the Math Department of the University of Auckland. In 2015 she has been a Visiting Professor with the FU Berlin, and from 2011 to 2014 she has been a Privatdozentin with the Institute of Theoretical Physics at the TU Berlin, where she received the Diploma and Dr. rer. nat degrees in physics from the Department of Solid-State Physics, in 2000 and 2003, respectively. From 2001 to 2002, she was a Visiting Scholar with the Department of Material Science, University of Minnesota, Minneapolis, MN, USA. She received the Habilitation (Venia Legendi) degree from TU Berlin, in 2011. Her research interests include the modeling of semiconductor quantum-dot lasers, nonlinear laser dynamics, and control with optical feedback. She is an Editor of the book entitled Nonlinear Laser Dynamics - From Quantum Dots to Cryptography (Wiley, 2011) - the 5th volume of Reviews of Nonlinear Dynamics and Complexity.

Nina Owschimikow studied physics at the TU Darmstadt and received her diploma in 2002. After a period in the biomedical industry she returned to physics. She obtained a doctoral degree from FU Berlin in 2011 for studies of rotational coherence in gaseous nitrogen. Since 2011 she is affiliated with TU Berlin and since 2019 also with the Ferdinand-Braun Institut für Höchstfrequenztechnik. Her present research interests are ultrafast optical spectroscopy and its application to 2D semiconductor materials.

1077-260X (c) 2019 IEEE. Personal use is permitted, but republication/redistribution requires IEEE permission. See http://www.ieee.org/publications_standards/publications/rights/index.html for more information.